

†Electronic Supplementary Information

Resilient Hollow Fiber Nanofiltration Membranes Fabricated from Crosslinkable Phase-Separated Copolymers

Michael P. Dugas,[†] Graham van Every,[‡] Bumjun Park,[†] John R. Hoffman,[†] Ryan LaRue,[‡] Aaron M. Bush,[†] Yizhou Zhang,[†] Jennifer Schaefer,[†] David Latulippe,[‡] and William A. Phillip^{†,}*

[†]205 McCourtney Hall, Department of Chemical and Biomolecular Engineering, University of Notre Dame, Notre Dame, Indiana 46556

[‡]1280 Main Street West, Department of Chemical Engineering, McMaster University, Hamilton, Ontario, Canada L8S 4L7

* To whom correspondence should be addressed: wphillip@nd.edu

This supplementary information contains detailed materials and methods, schematics of the hollow fiber modules, additional SEM micrographs, ¹H-NMR and GPC copolymer analysis, transport analysis of flat sheet membranes, FTIR and XPS analysis of the membrane functionalization reaction, pH responsive MgCl₂ rejection, and AFM analysis of membranes.

1: Detailed Materials and Methods.....	S2
2: Copolymer Characterization.....	S13
3: Flat Sheet Membrane Characterization.....	S15
4: Hollow Fiber Membrane Characterization.....	S19
5: Membrane Functionalization & Characterization.....	S22
6: Hindered Transport Calculations.....	S25
7: Chlorine and Solvent Exposure Characterization.....	S27
8: References.....	S34

1: Detailed Materials and Methods

1.1 Materials

All chemicals used in this study were purchased from Sigma-Aldrich unless noted otherwise. Trifluoroethyl methacrylate (TFEMA), oligo(ethylene glycol) methyl ether methacrylate ($M_n = 500$) (OEGMA), and glycidyl methacrylate (GMA) were the monomers used to fabricate the copolymer. Azobis(isobutyronitrile) (AIBN) was used as a radical initiator. Sucrose as well as 1.1, 2.1, 4.0, 6.0, and 19.0 kg mol⁻¹ poly(ethylene oxide) (PEO) purchased from Polymer Source, Inc. were utilized for solute rejection experiments. The dispersity (D) for each polymer, as reported by the manufacturer, was 1.03. Sodium chloride (NaCl), magnesium chloride (MgCl₂), sodium sulphate (Na₂SO₄), and magnesium sulphate (MgSO₄) were used for salt rejection experiments. Ethanol (200 proof) and a sodium hypochlorite solution (4.00-4.99% available chlorine) were purchased for solvent exposure and chlorine resistance experiments. NF90 and DK thin film composite membranes from Dow Water & Process Solutions and Suez Water Technologies, respectively, were used as benchmarks for the chlorine resistance of commercially-available nanofiltration membranes. 18 M Ω deionized water (Milli-Q) from a Milli-Q Advantage A10 filtration system was utilized for the hydraulic permeability measurements and the preparation of all aqueous solutions.

1.2 Synthesis and Characterization of P(TFEMA-OEGMA-GMA)

The poly(trifluoroethyl methacrylate-*co*-oligo(ethylene glycol) methyl ether methacrylate-*co*-glycidyl methacrylate) [P(TFEMA-OEGMA-GMA)] copolymer was synthesized through a free-radical copolymerization mechanism. Before the reaction, each monomer was purified of inhibitors by passing them through basic alumina columns. 0.5% AIBN (by moles of monomers) was dissolved in 15 grams of toluene contained in a three-port round bottom vessel. Once the

AIBN was dissolved, 4 g of TFEMA, 4 g of OEGMA, and 2 g of GMA were added to the solution. A stir bar along with a nitrogen inlet and gas outlet were added to the reaction vessel after the monomers. The solution was degassed with flowing nitrogen for approximately 20 min at room temperature. Then, the vessel was placed in an oil bath at 60 °C for 20 hours. The headspace in the vessel was purged with nitrogen gas throughout the polymerization. After the allotted time had elapsed, the vessel was allowed to cool to room temperature. The polymer solution was then added dropwise into hexane to precipitate the copolymer. The copolymer was redissolved in chloroform and precipitated in hexane to remove the unreacted monomer and dried in a vacuum oven. This procedure was repeated twice. After the final precipitation, the polymer was dried under vacuum for 24 h. Prior to membrane casting, the copolymer was stored in a sealed glass container. Analysis of the copolymer through hydrogen nuclear magnetic resonance spectroscopy (¹H-NMR), differential scanning calorimetry (DSC), and gel permeance chromatography (GPC) followed the same protocol as reported in previous work.¹

1.3 Flat Sheet (FS) and Hollow Fiber (HF) Membrane Preparation

1.3.1 Membrane Casting Solutions and Casting Conditions

The P(TFEMA-OEGMA-GMA) copolymer was added to solvent at a prescribed weight percent and stirred until a homogenous, transparent solution was generated. Once dissolved, the solution was passed through a 1- μ m glass syringe filter from Pall Corporation to remove any particulate. The filtered solution was then allowed to degas overnight prior to the membrane casting process. All the membranes were fabricated using a nonsolvent induced phase separation method, which was executed in a fume hood within a climate-controlled room held between 21 to 24°C and a relative humidity of 30 to 60%.

1.3.2 FS Sheet Blade Cast Membranes

To fabricate the FS membranes, an aliquot of casting solution was placed on a poly(vinylidene difluoride) (PVDF) substrate (Nanostone Water, Inc., PV400 ultrafiltration membrane). A doctor blade set to 63 μm above the substrate was utilized to apply an even layer of casting solution. Subsequently, the solvent was allowed to evaporate for a given period of time ranging from 0 to 5 minutes before the thin film of solution and substrate were plunged into a nonsolvent, either isopropanol or hexane, bath. The solvent-nonsolvent pairing and evaporation time were varied systematically to determine viable casting conditions.

1.3.3 HF Dip Coated Membranes

HF PVDF membranes, provided by The Dow Chemical Company, with an inner diameter of approximately 0.6 mm, an outer diameter of approximately 1.2 mm, and 30 nm nominal pore size were used in the fabrication of the HF membranes. The HF substrates were soaked in ethanol for 30 minutes to remove any pore stabilizing agents and debris from the surface. After the substrate was dried completely at room temperature and ambient pressure, the HF membranes were fabricated by pulling the substrate through a custom Teflon dye (Figure S1) containing an aliquot of casting solution. The Teflon dye was constructed such that the orifice at the bottom was within 30 μm of the diameter of the HF substrate to ensure that the casting solution remained within the dye while the membrane was cast. The solvent was then allowed to evaporate for a predetermined length of time before the fiber substrate was inverted and submerged into the nonsolvent bath at the same speed that it was pulled through the coating die. This casting process resulted in a uniform evaporation time over the whole length of the membrane leading to a consistent membrane.² The concentration of the copolymer in the casting solution and casting speed (simply determined using a timer in parallel with a ruler) were varied as follows.

Table S1: Copolymer HF casting conditions used to generate the membranes reported in Figure 3 of the main text.

Casting Solution Concentration [wt%] (Casting Speed: 0.5 cm s ⁻¹)	Casting Speed [cm s ⁻¹] (Casting Solution Concentration: 2 wt%)
2	0.25
4	0.5
6	1
8	1.5
10	2

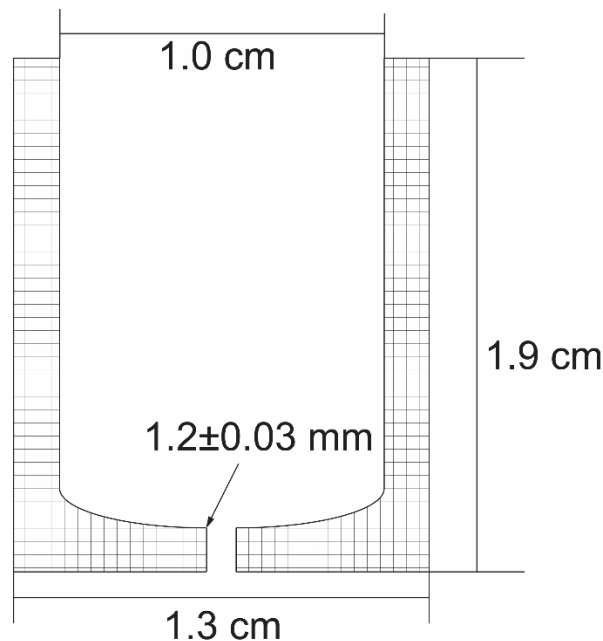


Figure S1: A schematic with measurements of the Teflon dye cross section. The orifice at the bottom of the dye was designed to be within 30 μm (0.03 mm) of the diameter of the HF substrate to ensure that the casting solution did not leak out of the dye during membrane casting. The schematic dimensions are not to scale.

1.3.4 Membrane Characterization Techniques

The surface and cross section morphologies of the membranes were imaged using scanning electron microscopy (SEM). A Magellan 400 field emission scanning electron microscope was used for this analysis. For surface characterization, approximately 1 cm² FS samples or 0.5 cm long HF samples were cut from larger membranes using a razor blade. Cross section samples of the membrane were prepared by submerging the samples in a liquid nitrogen bath until they thermally-equilibrated with the bath, and then breaking them. Samples were dried and mounted on

SEM pin stubs with carbon tape. The samples were kept dry during mounting and analysis occurred under vacuum. To prevent charging during analysis, the samples were sputter coated with 2.0 nm of iridium and grounded to the studs using colloidal silver emulsions. SEM micrographs were collected using an accelerating voltage of 5 kV and 6.3 pA current in immersion mode with a working distance of 4.0 mm.

Small angle x-ray spectroscopy (SAXS) was used to further characterize the structure of the membrane. FS membranes were cast onto Kapton film using the NIPS process described above and functionalized accordingly. The membranes were cut into thin sections that were placed into special glass capillary tubes purchased from Charles Supper Company. The tubes were either left dry, filled with water, or filled with ethanol before being sealed with epoxy. SAXS measurements were obtained using the Argonne APS synchrotron beamline 12-ID-B, operated by the Chemical and Materials Science group at Argonne National Laboratory, with an X-ray beam wavelength of 0.9322 Å (energy of 13.3 keV).

1.4 Membrane Functionalization and Characterization

Hexamethylene diamine or spermine was reacted to the epoxide moiety of the GMA repeat units using a ring opening reaction³ to charge-functionalize the copolymer membranes. Membrane samples were submerged in a 1 M aqueous solution of either hexamethylene diamine or spermine at room temperature. The membranes were allowed to react in the solution for 3 hours before being rinsed with water. Reacted samples were stored in water for future experiments.

The membrane functionalization reactions were characterized using attenuated total internal reflectance-Fourier Transform Infrared (ATR-FTIR) spectroscopy. Samples of the membranes were dried at room temperature in vacuum prior to FTIR analysis. Spectra were collected using a Jasco FT/IR-6300 spectrometer at wavenumbers from 650-4000 cm⁻¹ with a

resolution of 4 cm^{-1} . In addition, x-ray photoelectron spectroscopy (XPS) was conducted on reacted membrane samples. Membranes were dried under vacuum for 24 hours prior to analysis and staging on the sample holders. The sample holder was cleaned with methanol and allowed to dry for 15 minutes before use. Samples were placed on the sample holder and secured using double sided conductive carbon tape. Spectrum were collected using a PHI VersaProbe II spectrometer at 100keV. Spectrum were collected and analyzed using PHI Multipak.

The surface morphologies of unreacted and amine-functionalized membranes were examined using Atomic Force Microscopy (AFM). Micrographs were obtained using an Asylum MFP-3D FM with silicon nitride AFM tips suitable for liquid environment non-contact tapping analysis. The silicon nitride probe (PNP-TR, Nanoworld) had a resonance frequency of 17 kHz, spring constant of 0.08 N/m, and a length of 200 μm . Unreacted and amine-functionalized membranes were stored in water and ethanol prior to analysis. Before initiating analysis by AFM, the samples were removed from liquid storage and left to air dry for 2 minutes so that they could be affixed to a magnetic sample disk using double-sided tape. 100 μL of liquid was then placed on top of the sample in which the AFM probe was submerged. Surfaces were scanned over sample areas of $5 \times 5 \mu\text{m}^2$ at a scan rate of 0.5 Hz. Root-mean-square roughness was calculated for all images. Additional micrographs of the amine-functionalized membranes in ethanol were collected at scan areas of $1 \times 1 \mu\text{m}^2$.

1.5 Permeability and Solute Transport Experiments

1.5.1 Transport Testing Modules

FS membranes were tested in an Amicon 8010 stirred cell. One-inch diameter circular samples were cut using an arch punch and placed in the stirred cell with the copolymer material interfacing with the feed solution.

HF membranes were sealed into custom acrylic modules with 5-minute curing epoxy. One end of the HF was completely sealed while the other end was kept open to allow for the collection of the permeate. The module was designed for crossflow operation and was detailed in a previous study (Figure S2).² Some of the initial rejection experiments exhibited a low rejection of high molecular weight PEO samples. This observation led to a short investigation into how the HFs were secured in their module with epoxy. It was found that fully drying the sample lead to cracks at the epoxy-membrane interface. To address this issue, the period of time the membranes were left exposed to air was fixed at 20 minutes. This approach provided sufficient time for the epoxy to cure while keeping solvent evaporation to a minimum.

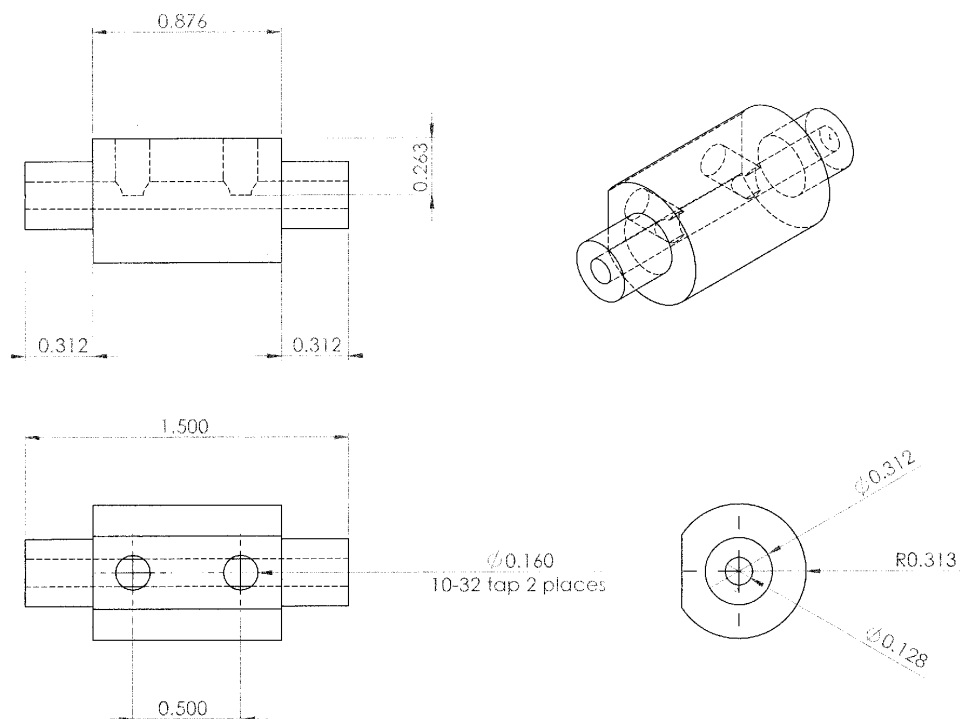


Figure S2: Multiview drawing of epoxy-sealed acrylic HF modules. The inlet and outlet seen on the flattened side of the module are threaded to allow barbed fittings to be screwed into place.

Several experiments, including the chlorine tolerance experiments, utilized a modification of the microscale, parallel-structured, crossflow filtration (MS-PS-CFF) system (Figure S3).⁴ The HF membranes were secured in filtration submodules designed to ensure easy collection of

permeate samples. Subsequently, the submodules were connected using tubing to complete the module. The transmembrane pressure in the modules was measured and maintained between 8-15 psig for each test. Plastic tubing was used to connect a feed reservoir to a gear pump drive, which was then connected to each filtration submodule. Plastic tubing was also used to connect the submodule back to the feed reservoir for retentate recycle. A flow meter was used to maintain the cross-flow rate at approximately 700 mL min^{-1} for rejection testing. The piping and instrumentation diagram is shown in Figure S4.



Figure S3: Photograph of the modified MS-PS-CFF system with appropriate connections and instrumentation attached.

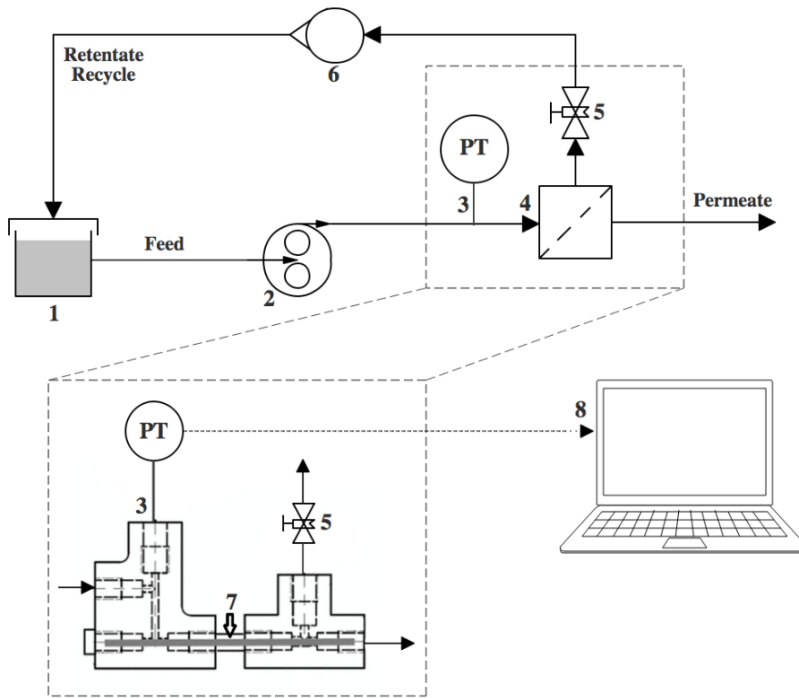


Figure S4: Piping and instrumentation diagram of the configuration used for hollow fiber membrane testing. The labelled components are as follows: (1) 1 L Feed Reservoir, (2) Gear Pump, (3) Pressure Transducer, (4) Filtration Module, (5) Needle Valve, (6) Rotameter, (7) Hollow Fiber Membrane, (8) USB connect to laptop for digital pressure measurement.

Both HF modules were attached to large reservoir tanks along with a Cole Parmer Model 75211-10 Gear Pump drive with a Micropump L21830 A-Mount Cavity Style Pump Head from Cole Parmer.

The hydraulic permeability of each membrane was quantified over applied pressures varying from 15 to 60 pounds per square inch for the acrylic modules utilizing Milli-Q water. The permeate solution was collected in a 20 mL vial that rested on a scale. At a fixed applied pressure, the mass of the permeate increased linearly over time. This relationship allowed for the water flux to be determined, which was then used to calculate the permeability according to Equation S1, where J_v is the volumetric permeate flux and ΔP is the transmembrane pressure:

$$L_p = \frac{J_v}{\Delta P} \quad (S1)$$

1.5.2 Solute Rejection Experiments

Aqueous solutions containing a single neutral solute (i.e., sucrose or a single PEO sample) at a concentration of 1 g L^{-1} were made for neutral solute rejection experiments. Milli-Q water was permeated through the membranes to ensure the membrane was rinsed of any previous solutions before each experiment. Once a rejection experiment was initiated, approximately 0.5 mL of solution was collected on the permeate side to ensure that the system had reached steady state. Then, two 0.5 mL samples were collected in 20 mL collection vials. Following the experiment, the membranes were permeated with water again to rinse any residual solution from the membrane. The vessels and test apparatuses were flushed thoroughly with Milli-Q water before testing the next solution. The concentration of solute in the permeate and feed solutions were analyzed using a Shimadzu TOC-L/TN Total Organic Carbon (TOC) system.

1.5.3 Ion Rejection Experiments

Aqueous solutions at a concentration of 1 mM were made for each salt: NaCl, MgCl₂, Na₂SO₄, and MgSO₄. The protocol for investigating the ion rejection followed the same procedure described in the previous section for neutral solutes. In these experiments, however, the concentration of solute in the permeate and feed solutions were analyzed with a Perkin Elmer Optima 3000 Induced Coupled Plasma-Optical Emission Spectrometer (ICP-OES). The samples were diluted to approximately 2 ppm with 3 vol% nitric acid. Calibration curves were run before each analysis ranging from 0 to 5 ppm.

Additionally, pH dependent ion rejection tests were conducted using 1 mM MgCl₂ feed solutions. The pH of these solutions was adjusted to a desired value between pH 2 to pH 11 using a 1 M solution of either hydrochloric acid or sodium hydroxide. The pH adjusted solutions were allowed to equilibrate overnight before experiments began. The procedure for permeate collection

and ion concentration characterization was the same as mentioned above. The membranes permeated approximately 0.5 mL of solution before any measurements were taken. The pH of the feed solution was measured before and after each experiment to ensure it remained constant.

1.6 Solvent and Chlorine Resistance Studies

The performance of the membranes before, during, and after exposure to a 90% (by volume) ethanol solution was examined to elucidate the solvent resistance of the membrane. Before each experiment, the membranes were permeated with an aqueous solution of 1 g L⁻¹ sucrose and 1 mM MgCl₂ to benchmark the permeability and solute rejection prior to testing. Afterward, the membranes were permeated with the ethanol solution for approximately 24 hours. Permeabilities were determined at different periods throughout the time interval to investigate if there was a change in the transport properties over the course of the study. After the allotted time elapsed, the membranes were transferred back to the aqueous solution to determine the permeability and rejection following exposure to the solvent. The membranes and apparatuses were cleaned with Milli-Q water after the experiment was complete.

In a similar manner, a 500 ppm solution of sodium hypochlorite at pH 8.4 was generated to examine the stability of the membrane in the presence of oxidizing agents. The membranes were placed into the MS-PS-CFF hollow fiber testing apparatus described above before experiments were conducted. The procedure described for accessing membrane stability to solvent exposure was also followed for exposure to hypochlorite. The hydraulic permeability as well as rejection of sucrose and MgCl₂ were measured prior to and following exposure to the chlorine solution. Afterwards, the membranes were permeated with ethanol to investigate the solvent resistance after exposure to hypochlorite. The membranes were then permeated with the aqueous solution to determine the transport properties following ethanol exposure.

2: Copolymer Characterization

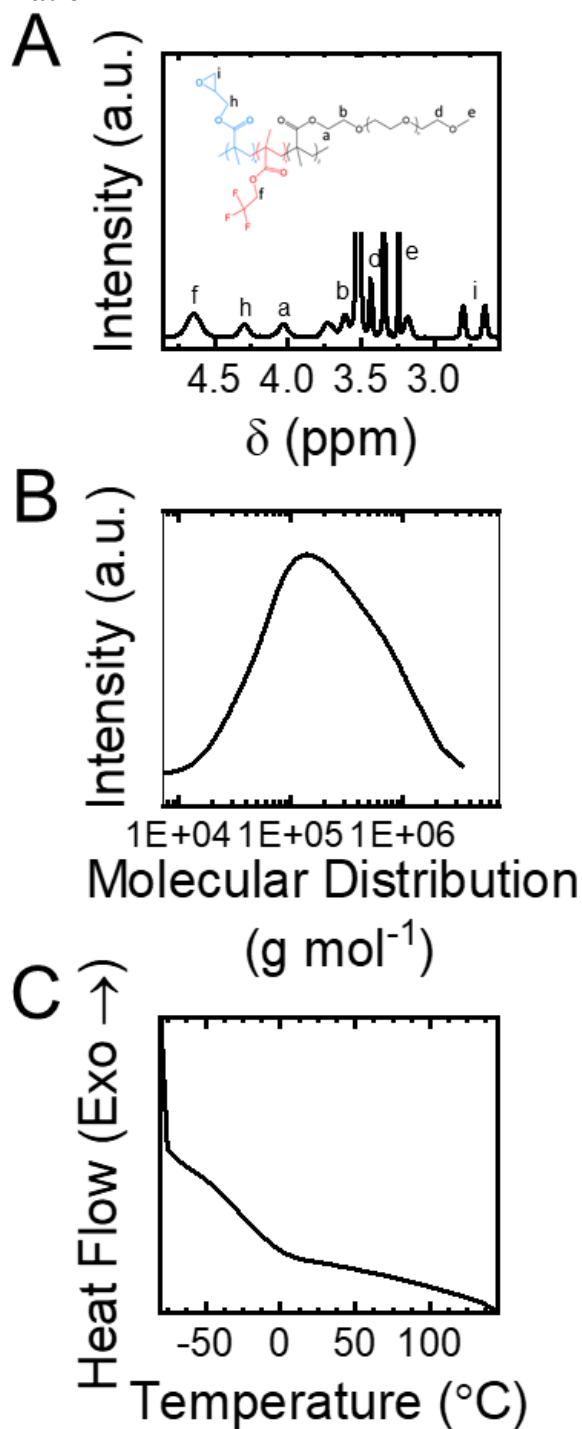


Figure S5: (A) ^1H -NMR spectrum of the P(TFEMA-*co*-OEGMA-*co*-GMA) copolymer material dissolved in deuterated DMSO. The peaks are labeled with the corresponding protons from each group on the structure provided. The peaks labeled **f**, **h**, and **a** were used to determine the composition of the copolymer. (B) GPC analysis of copolymer material dissolved in DMF. The eluent passed through the column at a flowrate of 1 mL min^{-1} , normalized by a toluene internal standard. The GPC was calibrated with poly(methyl methacrylate) standards. The analysis above

suggests a number-average molar mass of 103 kg mol^{-1} and a dispersity of 3.6. (C) DSC analysis of the copolymer material. The sample was heated at a rate of $10 \text{ }^\circ\text{C min}^{-1}$ and the reported data was collected during the second heating cycle. The scan exhibits only one glass transition temperature (T_g) at $-45 \text{ }^\circ\text{C}$. This transition temperature is consistent with the T_g of the OEGMA¹, suggesting that the OEGMA phase separates from the rest of the copolymer.

¹H-NMR was used to characterize the molecular structure and composition of the copolymers used in this study. The peaks of the spectrum in Figure S5A are labeled such that they correspond to the hydrogen(s) bonded at the labeled carbon atoms. The area under peaks **f**, **h**, and **a** were used to calculate the composition of TFEMA, GMA, and OEGMA in the copolymer, respectively. This analysis showed the average weight percent of each repeat unit to be $52.9 \pm 0.8\%$ TFEMA, $26.5 \pm 0.6\%$ OEGMA, and $20.6 \pm 1.5\%$ GMA.

The copolymer was also analyzed using GPC as shown in Figure S5B. The GPC used dimethylformamide (DMF) as the mobile phase and was calibrated with PMMA standards.¹ Using toluene as an internal standard, the molecular weight was determined to be $109 \pm 7 \text{ kg mol}^{-1}$ with a dispersity, $D = 4.8 \pm 1.5$.

DSC analysis was utilized to characterize the thermal transitions of the copolymer material. The copolymer was subjected to a range of temperatures from $-80 \text{ }^\circ\text{C}$ to $145 \text{ }^\circ\text{C}$ using a heating rate of $10 \text{ }^\circ\text{C min}^{-1}$. The data reported in Figure S5C was collected on the second heating cycle to ensure that the thermal history of the material would not interfere with the data analysis. One glass transition temperature (T_g) was observed at a temperature of $-45 \text{ }^\circ\text{C}$. This temperature coincides with the T_g of oligomeric ethylene glycol side chains of the OEGMA repeat units,¹ which suggests that the hydrophilic side chains phase separate from the rest of the copolymer. However, a T_g for the other components of the copolymer was not observed in the analysis. This absence could be due to thermal crosslinking of the GMA repeat units hindering the analysis.

3: Flat Sheet Membrane Characterization

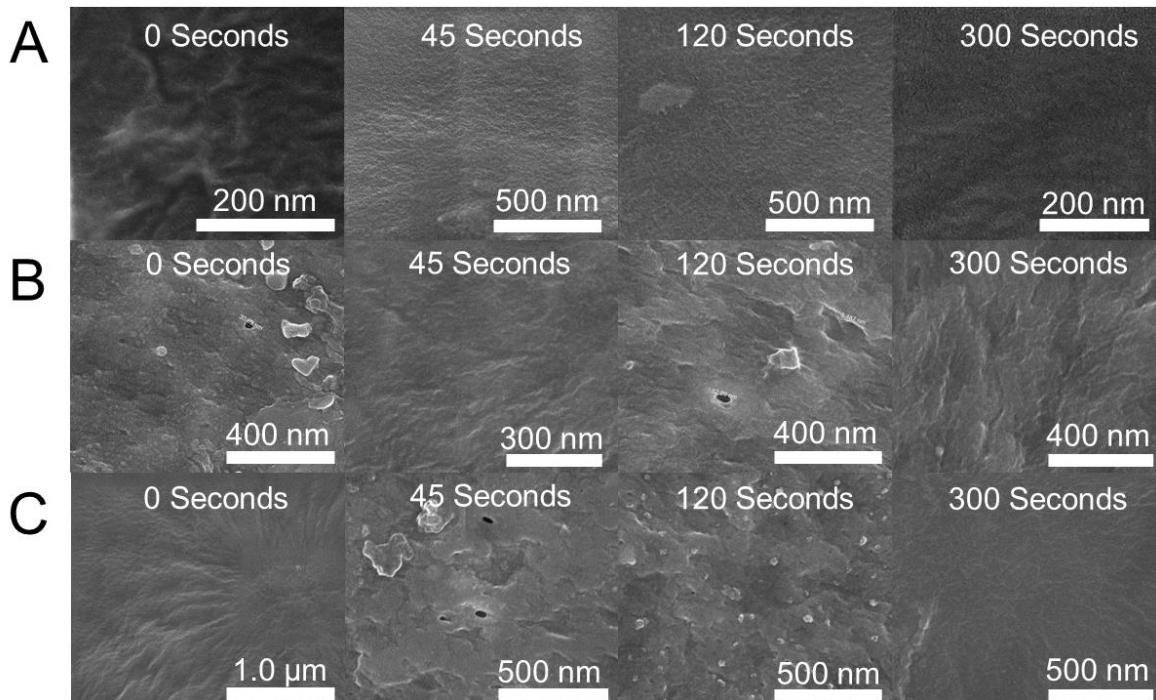


Figure S6: Surface SEM micrographs of FS membranes cast with (A) toluene, (B) DMSO, and (C) TFE using varied evaporation time. The micrographs indicate the formation of a dense layer for toluene and a decrease in defects with an increase in evaporation time for DMSO and TFE.

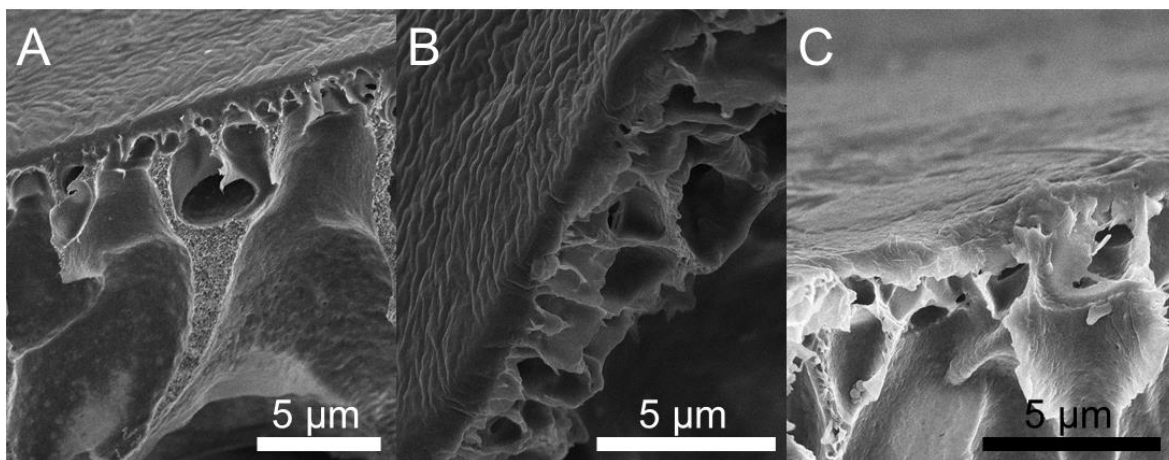


Figure S7: Cross section SEM micrographs of the FS copolymer membranes cast using (A) toluene, (B) DMSO, and (C) TFE as solvents. The micrographs show the deposited layer on the membranes.

A 10% (by weight) solution of copolymer dissolved in solvent was utilized to fabricate FS membranes. The viscosity of this solution allowed membranes to be cast in both the FS and HF

configurations. Three different solvent-nonsolvent pairings (i.e., toluene-hexane, DMSO-isopropanol, and TFE-isopropanol) were examined for casting in the FS configuration to determine the most viable pairing before proceeding to the fabrication of HF membranes. Varied evaporation times of 0, 45, 120, and 300 seconds were studied in the FS configuration to determine the time necessary for the fabrication of membranes without large pores or defects.

SEM analysis of the membrane surfaces (Figure S6) determined that the evaporation process affected each solvent-nonsolvent pairing differently. For toluene-hexane, the membranes showed no clear difference in surface structure as the evaporation time increased. This could be due to the high vapor pressure of the toluene leading to the rapid formation of a dense layer of polymer at the solution-air interface. For the DMSO and TFE systems, the membranes showed micron-scale defects on the surface at shorter evaporation times. This phenomenon is attributed to the lower vapor pressures of these two solvents compared to toluene. At short evaporation times, more solvent remains within the cast film of solution, which upon solvent-nonsolvent exchange with the isopropanol, leads to the formation of large pores on the membrane surface. The cross sections of selected membranes for each pairing are also shown (Figure S7). The membrane cast from toluene exhibits a dense layer directly on top of the PVDF substrate. This structure with no microporous layer indicates that the copolymer precipitated without undergoing a nonsolvent induced phase separation (NIPS) process. Conversely, the membranes cast from DMSO and TFE exhibit a thin, dense layer copolymer supported by a microporous layer. This asymmetric structure, which is mostly clearly observed in Figure S7C, is frequently observed in membranes made using the NIPS formation process.

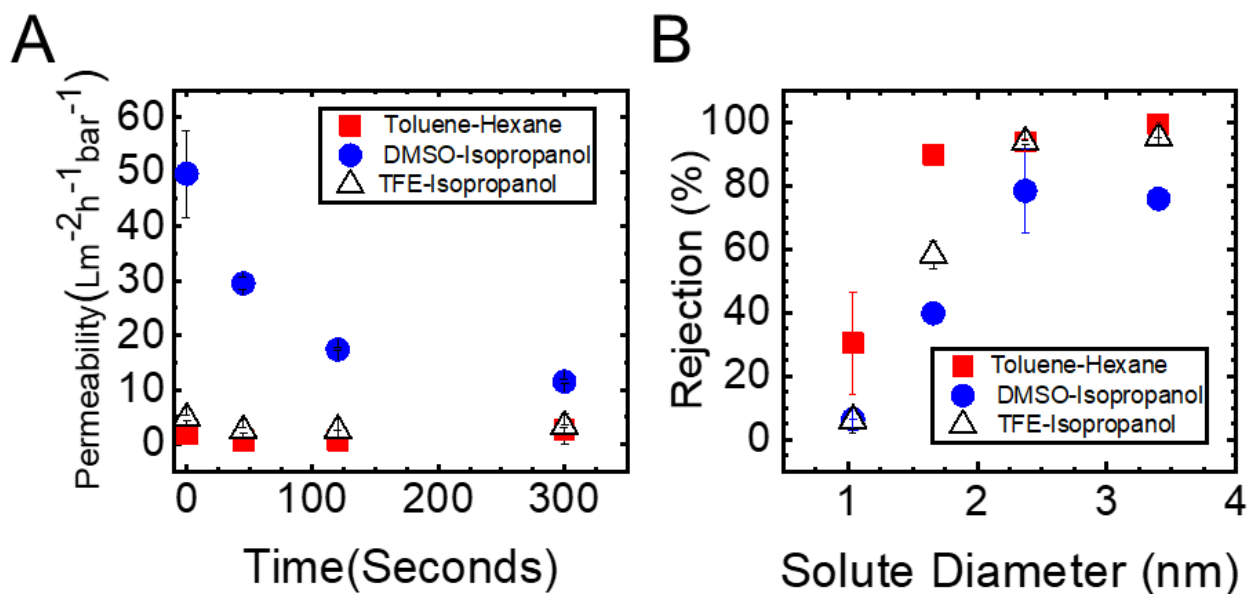


Figure S8: (A) Hydraulic permeability of FS membranes as a function of solvent evaporation time. (B) Neutral solute rejection curves for FS copolymers membranes. Rejection experiments were conducted using membranes fabricated with a 120 s solvent evaporation period for toluene-hexane and 300 s for the other two cases. The rejection values were calculated using the ratio of the solute concentration in the permeate to the solute concentration in the feed solution.

Once the membranes were fabricated, hydraulic permeability experiments were performed to investigate the effect of evaporation time on the performance of the membrane (Figure S8). For the toluene-hexane system, the permeability remained constant at $1.4 \pm 0.9 L m^{-2} h^{-1} bar^{-1}$. The nearly constant permeability is consistent with the rapid evaporation of toluene leading to a dense film. This hypothesis is further supported by the sharp rejection curve for membranes fabricated using this solvent-nonsolvent pairing. For the DMSO-isopropanol system, as the evaporation time increased, the permeability decreased from $49.6 \pm 7.9 L m^{-2} h^{-1} bar^{-1}$ to $3.2 \pm 0.2 L m^{-2} h^{-1} bar^{-1}$. The observed decrease in permeability can be rationalized by examining the SEM micrographs of the membrane surface, which demonstrate the formation of a dense active layer at longer evaporation times. A similar phenomenon was observed for the TFE-isopropanol system. This formation of a dense active layer, however, does not necessarily imply the formation of a continuous, defect-free active layer as demonstrated by the solute rejection curves in Figure S8B.

While the DMSO-isopropanol system exhibits a relatively sharp increase in percent rejection, the percent rejection did not approach 100% for solutes with larger diameters. In contrast, for the TFE-isopropanol system, the solute rejection curve is sharp and achieves nearly 100% rejection at larger solute diameters indicating the formation of an active layer without defects. Based on the results of the SEM micrographs, hydraulic permeability, and neutral solute rejection experiments, the TFE-isopropanol pairing with an evaporation time of 5 minutes was chosen for further experimentation with hollow fiber membrane formation. This choice was made because the SEM micrographs consistently demonstrated a continuous, intact active layer surface that corresponded to stable performance in permeability and solute rejection experiments.

4: Hollow Fiber Membrane Characterization

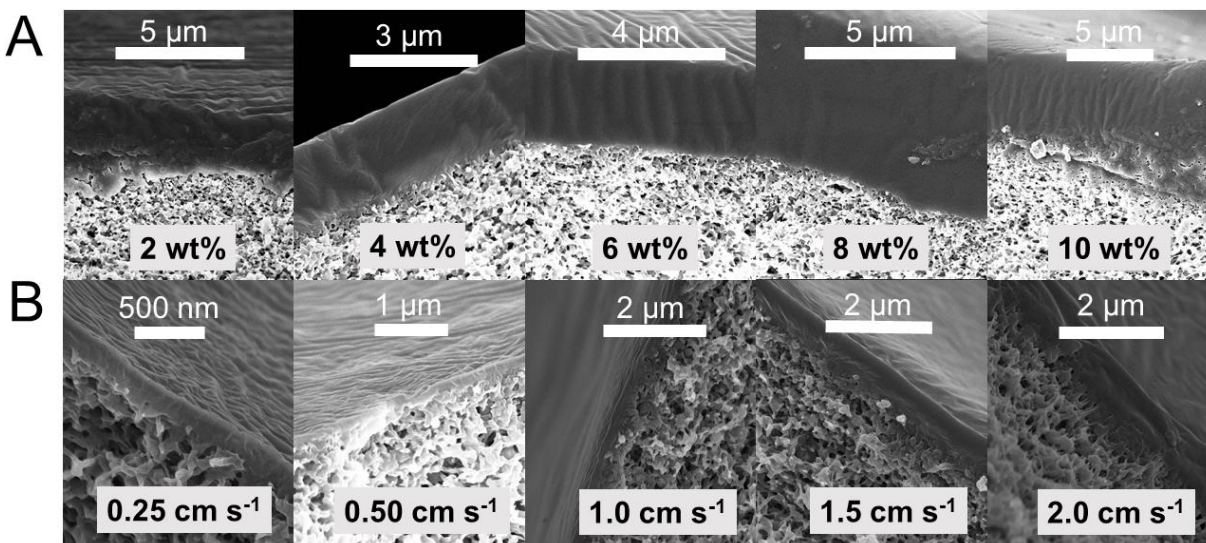


Figure S9: Cross section SEM micrographs of hollow fiber membranes as a function of (A) viscosity (for casting speed of 0.5 cm s^{-1}) and (B) casting speed (using a 2 wt% casting solution). The micrographs show with an increase in viscosity and casting speed increases the layer deposited on the membrane.

The influence of translation velocity and polymer concentration in the casting solution on the thickness of the layer deposited through dip-coating was studied using SEM microscopy. Figure S9 displays SEM micrographs of the cross-sections for membrane fabricated at each of the stated casting condition in Table S1. The micrographs moving across the row in Figure S9A demonstrate that as the concentration of the casting solution increases, the thickness of the deposited layer increases. The micrographs in Figure S9B also show that as the casting speed increases, the thickness of the deposited layer increases. The implications of these observations are reported in more detail in Figure 2 of the main text.

The hydraulic permeability of the composite membranes can be analyzed using a resistances-in-series model where the resistance of the HF composite membrane, $1/L_{p,c}$, is the sum

of the resistance from the PVDF substrate, $1/L_{p,s}$, and the resistance of the deposited copolymer active layer, $1/L_{p,a}$.

$$\frac{1}{L_{p,c}} = \frac{1}{L_{p,s}} + \frac{1}{L_{p,a}} = \frac{1}{L_{p,c}} = \frac{1}{L_{p,s}} + \frac{\ell}{L_{p,a}^*} \quad (\text{S2})$$

The resistance of the copolymer active layer is expected to scale with its thickness, ℓ . As such, the resistance of the deposited copolymer layer is written as the layer thickness over a constant, $L_{p,a}^*$, that is related to the solvent permeation mechanism through the copolymer layer. For example, if the pore walls were bare instead of being lined by PEO brushes, $L_{p,a}^*$ could be related to the porosity and pore diameter using the Hagen-Poiseuille relationship for pressure-driven flow. Based on the second form of Equation S2, Figure S10 displays the experimental resistances plotted versus the thicknesses of the copolymer layers as well as the line of best fit from linear regression.

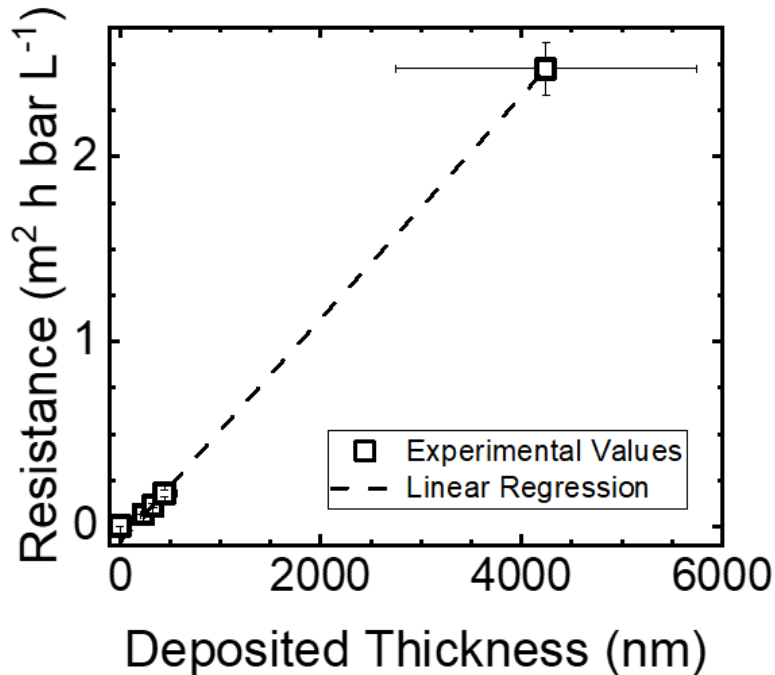


Figure S10: The hydraulic resistance of the composite HF membranes versus the thickness of the copolymer active layer. The errors of the experimental values are one standard deviation of $n = 3$ samples. The line of best fit was calculated using linear regression.

The hydraulic resistance of the composite membranes clearly scale linearly with the thickness of the active layer, which is consistent with the copolymer active layer being the dominant resistance to transport. The slope of the best fit line, corresponding to $L_{p,a}^*$, was calculated to be $6.03 \times 10^{-4} \pm 2 \times 10^{-6} \text{ m}^2 \text{ h bar L}^{-1} \text{ nm}^{-1}$. The y-intercept, which should correspond to the resistance of the PVDF substrate, was calculated to $-0.08 \pm 4 \times 10^{-3} \text{ m}^2 \text{ h bar L}^{-1}$. The resistance of the PVDF substrate based on experimental quantification of the hydraulic permeability was found to be $1.4 \times 10^{-3} \pm 4 \times 10^{-5} \text{ m}^2 \text{ h bar L}^{-1}$. An error propagation was conducted to determine if experimental measurement errors were causing the negative resistance and the discrepancy between the fit and expected values. This analysis suggests that the error in the intercept is expected to be $0.2 \text{ m}^2 \text{ h bar L}^{-1}$. Accounting for this error brings the fit values of the y-intercept well within range of the experimental resistance from the substrate.

5: Functionalization Characterization

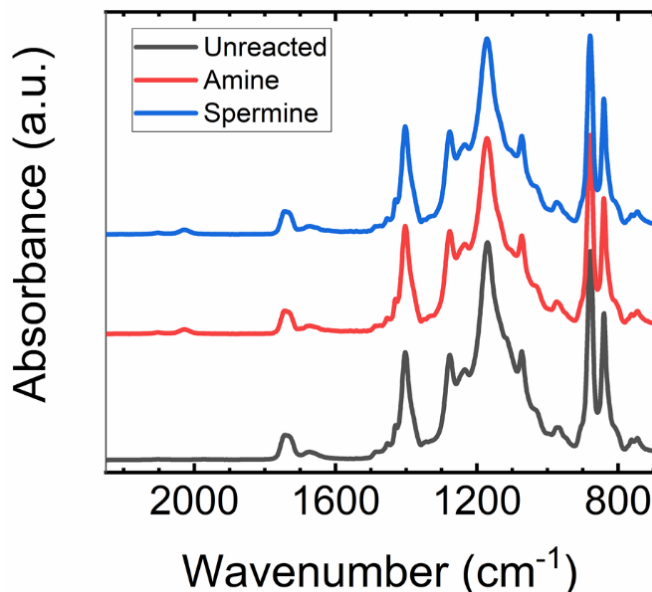


Figure S11: ATR-FTIR spectrum of the unreacted, amine-functionalized, and spermine-functionalized membranes. The spectra were normalized with the carbonyl stretching at approximately 1725 cm^{-1} . The epoxide shoulder peak at approximately 908 cm^{-1} was monitored to ensure complete reaction, followed by the appearance of peaks at approximately 1550 and 2000 cm^{-1} in the reacted membranes associated with the amine groups.

FTIR spectra were collected to provide an initial assessment of the functionalization reaction. Figure S11 displays the spectra from an unreacted membrane and two functionalized membranes. The unreacted membrane exhibits a small shoulder peak at approximately 908 cm^{-1} , indicating the presence of an epoxide ring. For the amine-functionalized and spermine-functionalized membranes, the disappearance of the peak at 908 cm^{-1} suggests an opening of the epoxide rings. While the appearance of peaks at approximately 1550 cm^{-1} and 2000 cm^{-1} suggest that the epoxide rings reacted with the hexamethylene diamine and spermine.

XPS analysis was utilized to further assess the progress of the functionalization reaction. Specifically, Figure S12 shows the XPS spectrum for the amine-functionalized membrane over a range of binding energies that correspond to nitrogen bonds. As shown, the collected spectrum can be modeled using two peaks that correspond to nitrogen binding at distinct energy states. These

peaks are associated with bonds formed by the primary amine that introduces positive charge within the pores of the membrane and the secondary amine that forms when the epoxide ring is opened to attach the amine to the pore wall. If the diamines reacted to just one epoxide ring, the peaks should have identical areas under them. However, the peaks are not identical in area and the peak at 401.1 eV, identified as the primary ammonium group, is notably smaller than the peak at 399.5 eV, which corresponds to the secondary amine.³ This imbalance suggests that both amines from many of the diamine molecules reacted with epoxide rings along the pore wall, thereby crosslinking the copolymer membrane.

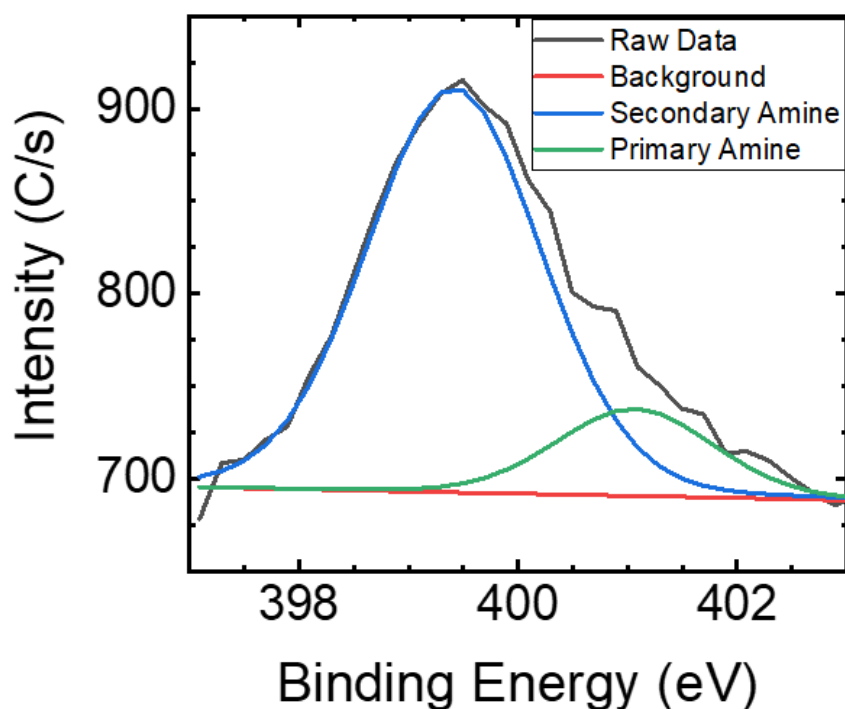


Figure S12: XPS spectrum of nitrogen peak with amine-functionalized membrane. The spectrum was shifted to the C-C peak at approximately 286 eV. The curves were fit using Phi MultiPak software.

Lastly, to establish the covalent attachment of amine functionality within the membrane pores, MgCl_2 rejection was quantified as a function of solution pH. Figure S13 summarizes the results of these experiments. From pH 3 to pH 11, the concentration of MgCl_2 in solution was kept

at 1mM. Over this pH range, MgCl_2 rejection remains constant at approximately 95% until the pK_a of the amine groups ($\text{pK}_a = 10.7$)¹ is approached. At a pH above the pK_a , the amines deprotonate and the electrostatic repulsion between the membrane and co-ions is dramatically reduced. As such, MgCl_2 rejection decreases to $22.4 \pm 0.6\%$ at pH 11. MgCl_2 rejection at pH 2 is lower because the concentration of MgCl_2 was increased to 10 mM to account for common ion effects that arise from adjusting the pH using hydrochloric acid. In the Donnan exclusion mechanism, as the ionic strength of the solution increases, the magnitude of the electrostatic repulsion between the membrane and co-ions is reduced due to screening of the surface charge. This manifests as the $44.3 \pm 1.9\%$ rejection of MgCl_2 at pH 2.

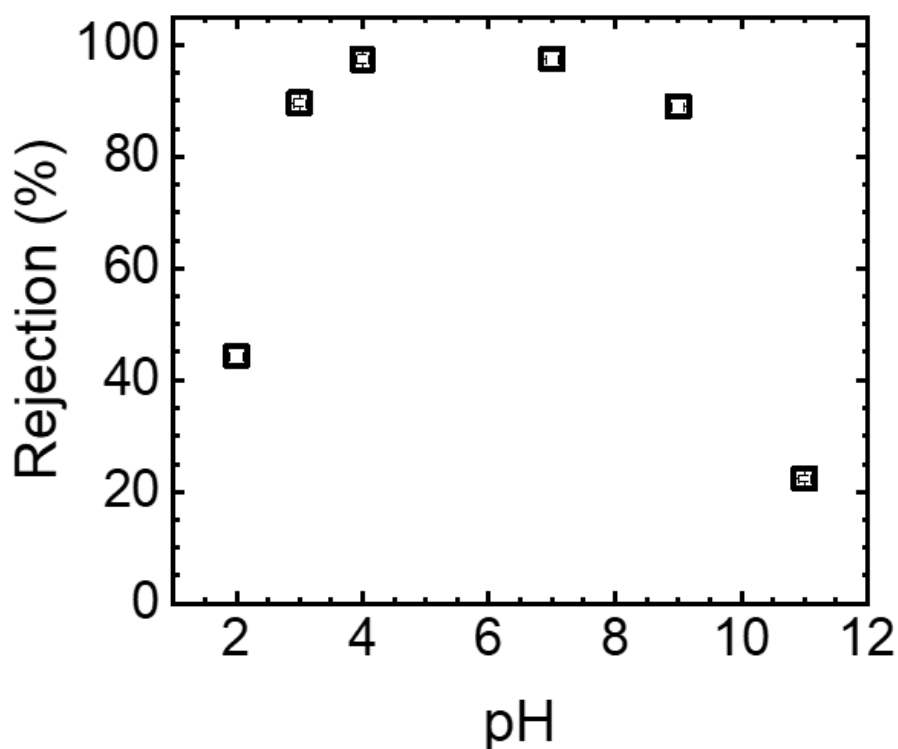


Figure S13: MgCl_2 rejections of amine-functionalized membranes as a function of pH. The cation concentration of permeate and feed solutions were calculated using ICP-OES. The pH was measured using a Fisher accumet AP115 portable pH meter equipped with an accumet 13-620-AP50A probe. The MgCl_2 concentration was 1mM except for the pH 2 solution, which was 10 mM, to account for common ion effect. The errors are one standard deviation.

Section 6: Hindered Transport Calculations

Neutral solute rejection experiments were conducted to determine the pore size of the copolymer membranes. The diffusion coefficient of the solutes, D , were found in the literature.⁵ Then, the Stokes-Einstein equation was used to relate the diffusion coefficient of the solute to its hydrodynamic radius in an aqueous solution, R_H , the viscosity of the solution, η , the temperature, T , and the Boltzmann constant, k_B .

$$D = \frac{k_B T}{6\pi\eta R_H} \quad (\text{S3})$$

The viscosity of the solutions was assumed to be equal to the viscosity of water at 22°C. The diffusion coefficient of the solute in the water was also used to calculate the mass transfer coefficient within the module using through a Sherwood number, Sh, correlation.

$$\text{Sh} = 0.022\text{Re}^{0.6}\text{Sc}^{0.33}$$
$$\frac{kd}{D} = 0.022 \left(\frac{dv^0}{\nu} \right)^{0.6} \left(\frac{\nu}{D} \right)^{0.33} \quad (\text{S4})$$

The correlation relates Sh to the Reynolds number, Re, and the Schmidt number, Sc.⁶ In this correlation, the Reynolds number is characterized by the superficial velocity of water, v^0 , tangential to the membrane surface, ν is taken as the kinematic viscosity of water, and the diameter of the membrane, d , is used as the characteristic length. The same diameter was used to calculate the Sherwood number, and ultimately, the mass transfer coefficient, k .

The mass transfer coefficient determined from the Sherwood number correlation can be used in conjunction with a thin film theory for concentration polarization to relate the observed sieving coefficient, S_o , to the actual sieving coefficient, S_a .⁷

$$S_o = \frac{S_a}{(1 - S_a) \exp\left(\frac{-Jv}{k}\right) + S_a} \quad (\text{S5})$$

S_o is calculated as the ratio of the solute concentration in the permeate solution to the solute the concentration in the feed solution; S_a is calculated as the solute concentration in the permeate solution over the solute concentration at the solution-membrane interface on the feed side.

The percent rejections values, R , used to construct the rejection curve were calculated using the relationship between the rejection and the sieving coefficient:

$$R = (1 - S) \times 100\% \quad (\text{S6})$$

Once the influence of concentration polarization is considered, the actual rejection, $R_a = 1 - S_a$, can be expressed using a theory for hindered transport developed by Zeman and Wales (Equation S6)⁸, which relates the sieving coefficient to the ratio of solute radius to pore radius, λ .

$$1 - R_a = \{1 - [\lambda(\lambda - 2)]^2\} \exp(-0.7146\lambda^2) \quad (\text{S7})$$

Using this method, the pore size of the copolymer membranes can be estimated.

Section 7: Chlorine and Solvent Exposure Characterization

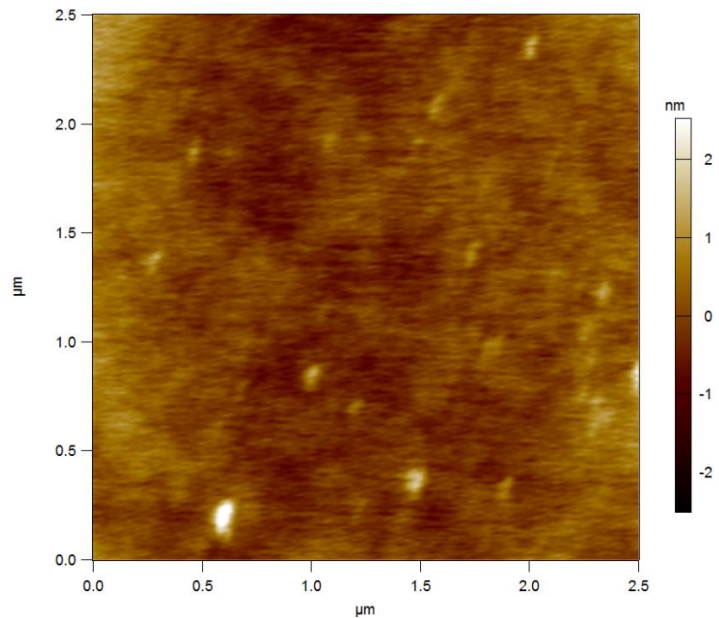


Figure S14: AFM micrograph of unreacted copolymer membrane in a dry state.

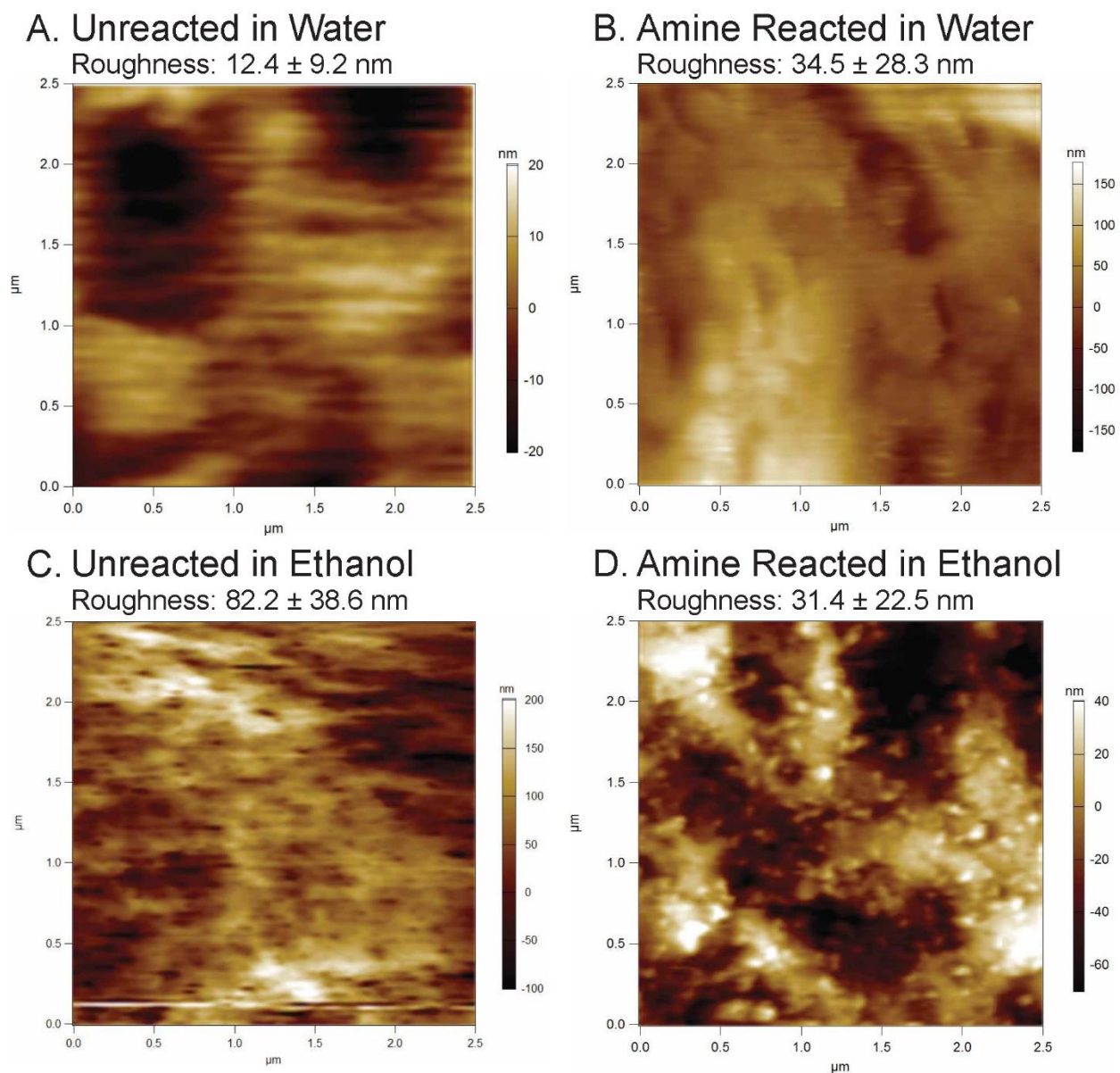


Figure S15: AFM image of (A) unreacted membrane soaked in water, (B) amine-functionalized membrane in water, (C) unreacted membrane in ethanol, and (D) amine-functionalized membrane in ethanol.

As shown in Figure S14, the surface of the dry membrane sample is featureless and smooth with a low variation in sample height across the surface. Subsequently, the surfaces of unreacted and amine-functionalized FS copolymer membranes were characterized in water and ethanol environments using AFM analysis (Figure S15). Multiple attempts were made to maximize the interaction between the AFM tip and the membrane surface during analysis. However, it is

postulated that interactions at the membrane surface within the aqueous environment made engaging the AFM tip with the surface more difficult leading to poor trace-retrace being observed during imaging. As such, the micrographs in Figure S15A and S15B depict the highest resolution achieved when testing within water. Using ethanol, the liquid droplet spread across the surface and proper non-contact mode tip engagement was more readily achieved. This is highlighted by the increase in resolution observed in Figure S15C and S15D.

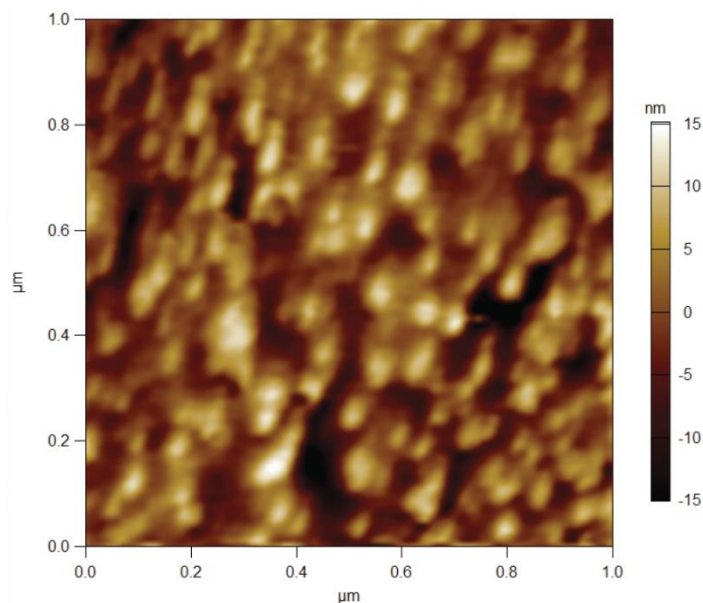


Figure S16: Higher resolution AFM micrograph of the amine-functionalized copolymer membrane in ethanol. The formation of nodules can be seen as the white regions on the surface.

For the unreacted membranes, exposure to water shows a relatively featureless membrane with a low surface roughness. Once the unreacted membrane was exposed to ethanol, however, the surface roughness increased dramatically, which suggests the membrane surface may have rearranged in the presence of ethanol. For the amine-functionalized membrane, the water-swelled and ethanol-swelled membranes have nearly identical roughness measurements. The similar measurements suggest that membrane surface is not irreparably harmed by the presence of the solvent. Instead, in the ethanol environment, nodules form on the surface of the membrane, as can

be seen by comparing Figure S15B and S15D. A higher resolution micrograph of an amine-functionalized membrane in ethanol highlighting these nodules is provided as Figure S16. The characteristic size of these nodules is commensurate with the larger characteristic length identified from the SAXS spectrum, which suggests that the nodules maybe micelles that fixed on the membrane surface but that cannot escape due to the crosslinked copolymer structure. The combination of results from SAXS, AFM, and transport analysis demonstrate that the amine-functionalized membranes are resistant to ethanol exposure, likely due to crosslinking in the membrane.

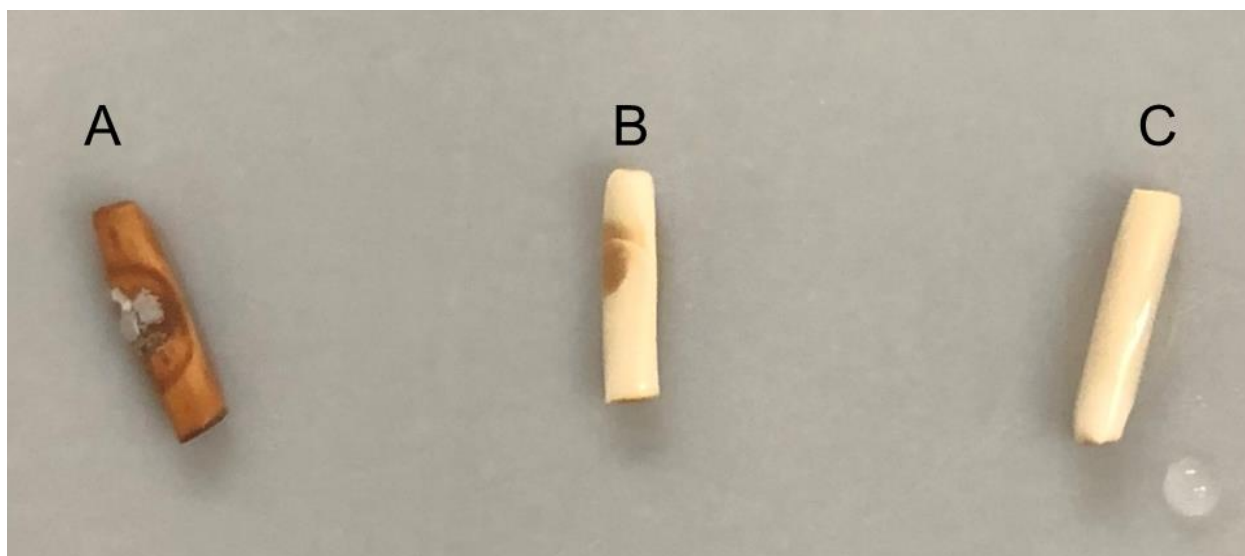


Figure S17: Photographs of (A) an amine-functionalized membrane prior to exposure to a 500 ppm hypochlorite solution, (B) an amine-functionalized membrane after exposure to a 500 ppm hypochlorite solution, and (C) an amine-functionalized membrane after exposure to a 500 ppm hypochlorite solution and ethanol.

Chlorine resistance experiments were conducted to evaluate the effects of oxidizing agents, such as the hypochlorite ion, on membrane performance. While conducting the experiments, the membranes exhibited a color change from a dark brown to a cream color, as shown in Figure S17A and S17B, respectively. This change, along with the drop in MgCl_2 rejections, suggested that a chemical reaction may have taken place, which prompted the ethanol permeation experiment

following chlorine exposure. If the amine moieties, the membrane should remain intact in an ethanolic environment. Although the membrane never regained its color, as shown in Figure S17C, the hydraulic permeability remained constant and the salt rejection recovered to approximately its initial level following exposure to ethanol and subsequent exposure to water. The fluctuation in salt rejection led to the hypothesis that chloramines were being formed as the hypochlorite reacted with the primary amines within the membrane. This reaction would neutralize the positive surface charge and temper the Donnan exclusion mechanism. ATR-FTIR analysis was conducted to evaluate this hypothesis. Figure S18 shows the shift of the amine peak at 1570 cm^{-1} to 1540 cm^{-1} , indicating that the chloramine moiety had been formed.⁹ However, after the permeation in ethanol, the amine peak shifts back to approximately the original position, indicating the chloramine bond was no longer present.

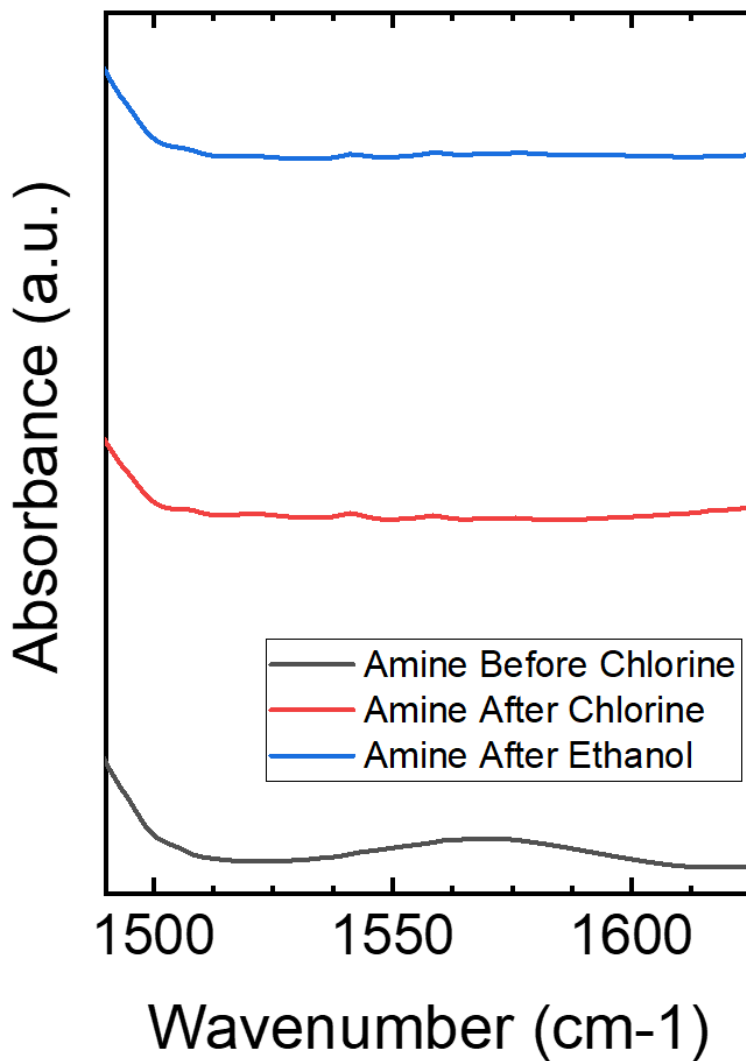


Figure S18: ATR-FTIR spectrum of the amine-functionalized membrane before exposure to hypochlorite, after exposure to hypochlorite, and after soaking the membrane in ethanol following exposure to hypochlorite. The spectra were normalized to the peak at approximately 1725 cm^{-1} . The shift in the amine peak at approximately 1570 cm^{-1} to 1540 cm^{-1} is consistent with the formation of chloramine bonds upon while the shift back following exposure to ethanol reveals the chloramine bonds are no longer present.

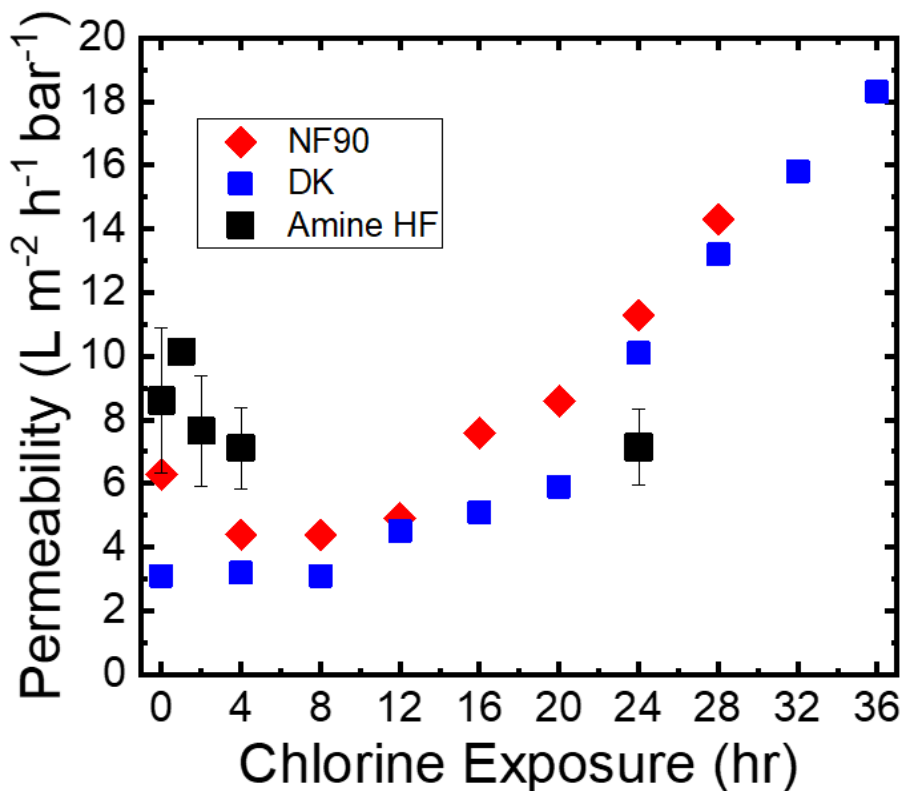


Figure S19: Comparison of amine-functionalized HF membrane to commercial FS membranes with chlorine exposure. The commercial membranes are one-time measurements, so therefore do not have associated errors. The HF membranes errors are one standard deviation of four samples.

Despite the formation of chloramines, the amine-functionalized HF membrane proved to be resistant to structural degradation by chlorine. To further highlight this nanostructural stability, a comparison of the HF copolymer membrane to commercially available thin film composite (TFC) NF membranes was conducted. Figure S19 compares the hydraulic permeability of the two commercial NF membranes, NF90 and DK, and the amine-functionalized HF membrane versus time in a 500 ppm chlorine solution. The hydraulic permeability of the HF membrane is initially higher than that of the commercial membranes and its value remains constant over the course of the experiment. In contrast, the hydraulic permeability of the NF90 and DK membranes increase dramatically at longer times due to structure degradation of the TFC NF membranes.

8: References

- 1 S. Qu, T. Dilenschneider and W. A. Phillip, *ACS Appl. Mater. Interfaces*, 2015, **7**, 19746–19754.
- 2 Y. Zhang, R. A. Mulvenna, B. W. Boudouris and W. A. Phillip, *J. Mater. Chem. A*, 2017, **5**, 3358–3370.
- 3 R. Barbey, V. Laporte, S. Alnabulsi and H. A. Klok, *Macromolecules*, 2013, **46**, 6151–6158.
- 4 A. S. Kazemi, B. Patterson, R. J. LaRue, P. Papangelakis, S. M. Yoo, R. Ghosh and D. R. Latulippe, *Sep. Purif. Technol.*, 2019, **215**, 299–307.
- 5 J. Shao and R. E. Baltus, *AIChE J.*, 2000, **46**, 1149–1156.
- 6 M. - C Yang and E. L. Cussler, *AIChE J.*, 1986, **32**, 1910–1916.
- 7 L. J. Zeman and A. L. Zydney, *Microfiltration and ultrafiltration: Principles and applications*, Marcel Dekker, 1996.
- 8 L. Z. Michael Wales, *Sep. Sci. Technol.*, 1981, **16**, 275–290.
- 9 M. J. Cran, S. W. Bigger and S. R. Gray, *Desalination*, 2011, **283**, 58–63.